Reply to the reviewer comments
Manuscript se-2019-33

Dear Anke,

Thank you for your positive assessment of our work and for your constructive comments. Please find hereafter our answers to your comments.

Best regards,
The authors

Reviewer comments

1. *How true are the small scale structures in Fig. 3b?*

   The Manuscript-Figure 3 in is intended to present the qualitative difference between the velocity model resolution that can be obtained with FAT and FWI. Indeed, considering the huge jump in terms of the recovered details the question about their reliability is reasonable.

   Therefore in Górszczyk et al. (2017) we have spent significant efforts dedicated to validation of our FWI model. The QC was based on: (i) qualitative and quantitative assessment of the real-vs-synthetic data fitting using Dynamic Image Warping (DIW, Hale, 2013); (ii) geophone response estimation (i.e. source wavelet estimation within the framework of source-receiver reciprocity); (iii) phase interpretation via ray-tracing; (iv) chequerboard tests of different scales.

   To recall some of the results of our QC (exhaustive discussion is provided in Górszczyk et al. (2017)) in Figure 1 we present the accuracy of data-fitting between the observed and synthetic data, generated in FAT and FWI models. From the zoom-insets in Figure 1(ab) it is clear that FWI drives the interleaved wiggles, which are not aligned in case of data generated in the initial model (Figure 1(a)), into their correct position (Figure 1(b)). The same consistency is also visible for the amplitude trends (Figure 1(d).

   To quantitatively express this accuracy we utilize DIW. In Figure 2(ab) we present the estimated local time-shift panels for the single OBS as well as for the whole dataset. Histogram of shifts presented in the inset and Figure 2(c) shows that vast majority of the time-shifts fall between ±30 ms which gives us an idea about the reconstruction accuracy.

   Moreover, in the presented manuscript we further extensively validate both FAT and FWI models against the separate dataset and the different velocity model-building (namely Slope Tomography) and depth imaging (namely Kirchhoff PSDM) techniques.

   Combing all the information from the previous and current exercises we can conclude, that the fine structures in the FWI model are explained by the seismic data, and therefore are related to the underlying structure. While it is true that in the areas of poor illumination (flanks and the deepest parts of the model) the uncertainty of the reconstruction increases.

2. *A Fig. 3c showing plain MCS data or MCS data overlaid by the transparent FWI velocity field, could be useful for the reader.*

We understand the usefulness of such comparison, therefore we perform it directly in Manuscript-Figure 8. Also 'clear' PSMD section is presented in Manuscript-Figure 7a. Therefore, to avoid repetitions of the same content along the manuscript we prefer to keep the Manuscript-Figure 8 unchanged.

3. *For presenting seismic velocity fields gained by traveltime modelling it is common to show an image of a resolution test.*

We agree that the chequerboard resolution tests (although being pure inverse-crime tests) are quite commonly used for approximation of the structural correctness of the smooth tomographic model - especially when these model are a subject to further geological interpretation.

In our case, rather than focusing on building the FAT model which is as detailed as possible, we follow Ockham's razor rule - namely we build the model as smooth as possible, which explains the traveltimes within the error avoiding cycle-skipping criteria during FWI. This is because our aim was to introduce the structure in the final model *via* FWI and not FAT.

Of course, it does not mean that we skip QC of the FAT model. We focus on the validation of the FAT model through the traveltime- and seismic data-fitting. Indeed, due to the ultra-long offset, the traveltimes are long, leading to a large number of wavelengths to propagate. This in turn, causes higher possibility to accumulate the traveltime error and fall into the cycle-skipping from the very beginning of subsequent FWI (Pratt, 2008). In Górszczyk et al. (2017) we describe in details the procedure behind building the FAT model - based on the iterative, model driven refining of the picked first breaks.

To shed some light about the accuracy of traveltime-fitting provided by our FAT model, in Manuscrip-Figure 2(b) we overlay on the OBS gather the picked and calculated first-arrival traveltimes. Here in Figure 3 we present the synthetic OBS gather generated in the FAT model with superiposed curves corresponding to picked (red) and calcualted (green) first-break traveltimes. As can be seen both lines follows quite accurately the first arrival signal. Indeed at very far offset the accuracy decreases, as a result of lack of OBS coverage in this area - which was fairly pointed in one of your further comments. The two bottom panels show the overall distribution of traveltime mismatch, which in average is below 50 ms.

Therefore, we believe that with traveltime error at this level our smooth FAT model is robust - since we did not observe cycle-skipping problem during early stage FWI. Moreover, the PSDM results inferred from FAT model, provide additional benchmark confirming its robustness.

4. *The low velocity zone (LVZ) (in Fig. 3b) in the west (15-35 km profile distance and 15 km depth) does look like an artefact. How robust is the LVZ between 35-50 km profile distance at 10 km depth*

The first LVZ (15-35 km profile distance and 15 km depth) is most likely an artefact. It is located at the edge of the illumination from the landward side of the profile and due to the lack of constraint from the other side we are introducing some smearing-like anomalies. In the updated version of the Manuscript-Figure 3, we provide the first-arrival ray-coverage mask - which was also suggested by the Reviewer 1 - to better emphasize the illumination of the model space by the data. We also point out that the perturbations at the edge of the ray-coverage might be artificial.

The second LVZ (35-50 km profile distance at 10 km) is better sampled by the data and therefore we believe this is the geological feature. Its existence in this area causes quite complex propagation of the wavefield which is evident from the OBS gathers (for example complex package of arrivals between 20-35 km in Figure 1(c)).

Moreover in Figure 4 focusing of the PSDM section derived from FWI model (containing LVZ) and FAT model (no sharp LVZ) is better in this particular area. It is also worth to mention that existence of similar features were reported by in the western part of the Nankai Trough (Park et al., 2010; Kamei et al., 2012)

5. *Figure 3 shows that only 100 km of the profile is covered by OBS. This means we would expect a rather bad resolution at the profile with distances larger than 100 km. By that I would be careful with the low velocity zone found in this portion of the model.*

We agree with your statement. We avoid over-interpretation of the velocity model in the area located near to the the ends of the OBS profile - even-though the area around 100 km of the profile is still relatively well constrained through the undershooting of the wavefield propagating in the upper mantle. However, based on the results (e.g. Kodaira et al., 2003) (derived from the complementary OBS profile in the Tokai area), it is likely that another zone of lower velocities is located in in this region.

6. *How do the authors interpret the high positive velocity gradient directly on top of the subducting Moho? Underplating of the subducting plate? (Fig. 11b)*

In this case the change of the gradient shall be interpreted as a boundary itself (namely Moho) rather than some structure on top of Moho. The fact that it looks like a band of width of about 1-2 km is due to the decreasing resolution with increasing depth (in particular increasing velocity).

Considering Vp values of 8000 m/s, and taking into account that the highest effective frequency which we used during FWI was 8 Hz, the theoretical resolution (assuming omnidirectional coverage) is 500 m. In practice, due to the: (i) sub-horizontal propagation at this depth (scattering angles greater than 120 degrees); (ii) lack of clear short-spread PmP reflections; (iii) adaptive smoothing which is applied for regularization; (iv) and 2D reconstruction, this theoretical resolution has to be multiplied by at least factor of 2.

7. *Oceanic crust in general shows high lateral variation in composition and resulting seismic velocities. So, not necessarily a volcanic ridge is needed to explain the variations in the seismic velocity field at crustal level.*

We agree that the velocity variations in the subducting oceanic crust can have various origins e.g. different rock types combined with deformation. In Tokai area we can expect also the influence of the Izu Arc colliding with the central Japan as well as the initial thrusting stage around the Zenisu Ridge. We change the manuscript text accordingly to underline this information.

Nevertheless, there have been previous studies which were tackling the subject of geometry of the subducting plate and they suggested existence of horst-like structures (volcanic ridges) underneath the accretionary prism. Therefore it can be accepted to assume the existence of such ridges in this region. Moreover, fluid migration can occur along the ridge-bounding faults causing alternation of the deep rocks (e.g. serpentinization) which may actually affect the crustal velocity structure. Such fluid rock interaction and velocity alteration have been reported at the outer ridge of the Tohoku margin (Korenaga, 2017).

8. *In the section 3.2.4 "Backstop area" the authors state that they cannot put their results into the context with geologic studies. However, I think this section need to have a comparison to the*

findings of the original studies and their interpretation.

You are right that the results of our imaging can potentially bring new insight int the structure and evolution of the backstop in the Tokai segment. In case of geological interpretation, (for now) we are trying to avoid too much of speculations, which could distract the readers' attention from the main message of the paper, being more methodological in nature. We believe that to impose valid interpretation of the complex backstop area in this region we need to combine more data - coming not only form the field of seismic imaging (even-though reprocessing of the nearby OBS profile using FWI is now one of the ongoing works).

As we mentioned, the backtop in the Tokai segment is most likely the ancient accretionary prism covered by the sediments coming from the overriding plate, i.e. fore-arc basin. No active deformation can be clearly identified this area anymore - although the imprints of complex deformations is quite strong (the deformation is still active in the frontal area, (see Yamada et al., 2014)). In the more central part of the Nankai area, the Kumano fore-arc basin is such a typical example and the underlying old accretionary prism which is not actively deforming (Shiraishi et al., 2019).

References

Górszczyk, A., Operto, S., and Malinowski, M. (2017). Toward a robust workflow for deep crustal imaging by FWI of OBS data: The eastern Nankai Trough revisited. *Journal of Geophysical Research: Solid Earth*, 122(6):4601–4630.

Hale, D. (2013). Dynamic warping of seismic images. *Geophysics*, 78(2):S105–S115.

Kamei, R., Pratt, R. G., and Tsuji, T. (2012). Waveform tomography imaging of a megasplay fault system in the seismogenic Nankai subduction zone. *Earth and Planetary Science Letters*, 317-318:343–353.

Kodaira, S., Nakanishi, A., Park, J. O., Ito, A., Tsuru, T., and Kaneda, Y. (2003). Cyclic ridge subduction at an inter-plate locked zone off Central Japan. *Geophysical Research Letters*, 30(6):1339.

Korenaga, J. (2017). On the extent of mantle hydration caused by plate bending. *Earth and Planetary Science Letters*, 457:1–9.

Park, J. O., Fujie, G., Wijerathne, L., Hori, T., Kodaira, S., Fukao, Y., Moore, G. F., Bangs, N. L., Kuramoto, S., and Taira, A. (2010). A low-velocity zone with weak reflectivity along the Nankai subduction zone. *Geology*, 38(3):283–286.

Pratt, R. G. (2008). Waveform tomography - successes, cautionary tales, and future directions. In *Presented at the 70th Annual EAGE Conference & Exhibition, Roma*, pages WO11 – Full–Waveform Inversion: current status and perspectives.

Shiraishi, K., Moore, G. F., Yamada, Y., Kinoshita, M., Sanada, Y., and Kimura, G. (2019). Seismogenic zone structures revealed by improved 3d seismic images in the nankai trough off kumano. *Geochemistry, Geophysics, Geosystems*.

Yamada, Y., Baba, K., Miyakawa, A., and Matsuoka, T. (2014). Granular experiments of thrust wedges: Insights relevant to methane hydrate exploration at the nankai accretionary prism. *Marine and Petroleum Geology*, 51:34–48.
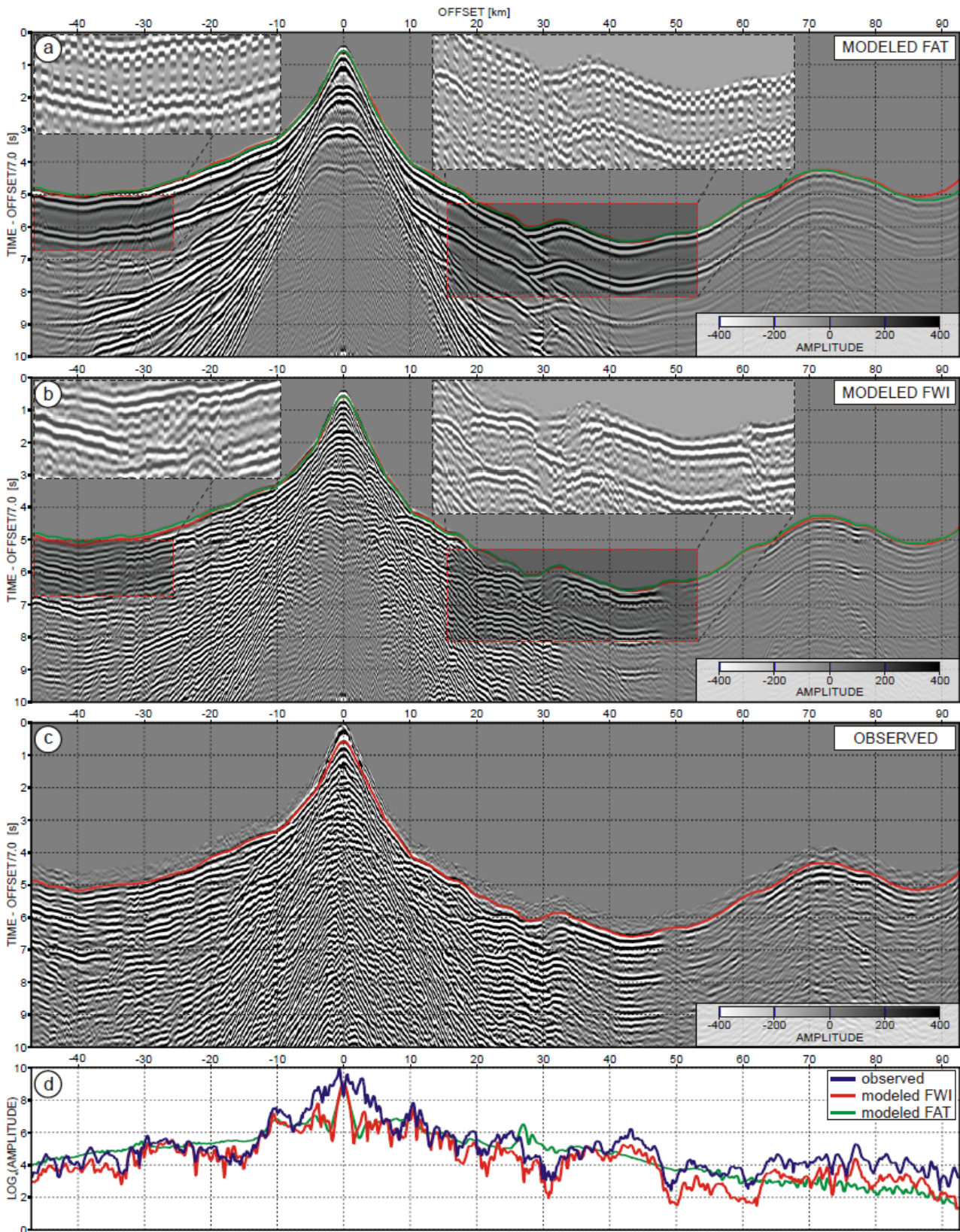
Figures

Figure 1: Comparison between the observed and modeled seismograms. (a-b) Synthetic data computed using the (a) FAT and (b) FWI models. (c) Observed data. Zoom-panels show 5 interleaved traces from modeled and observed OBS gathers. The red/green curves (a-c) represent the picked/calculated first-arrival traveltimes respectively using the (a) FAT and (b) FWI models. The true-amplitude seismograms in (a-c) are plotted using the same amplitude scale. (d) Comparison of the amplitude-versus-offset curves extracted from the seismograms shown in (a-c). The amplitudes are extracted from a 400 ms window after the first arrivals. From Górszczyk et al. (2017)
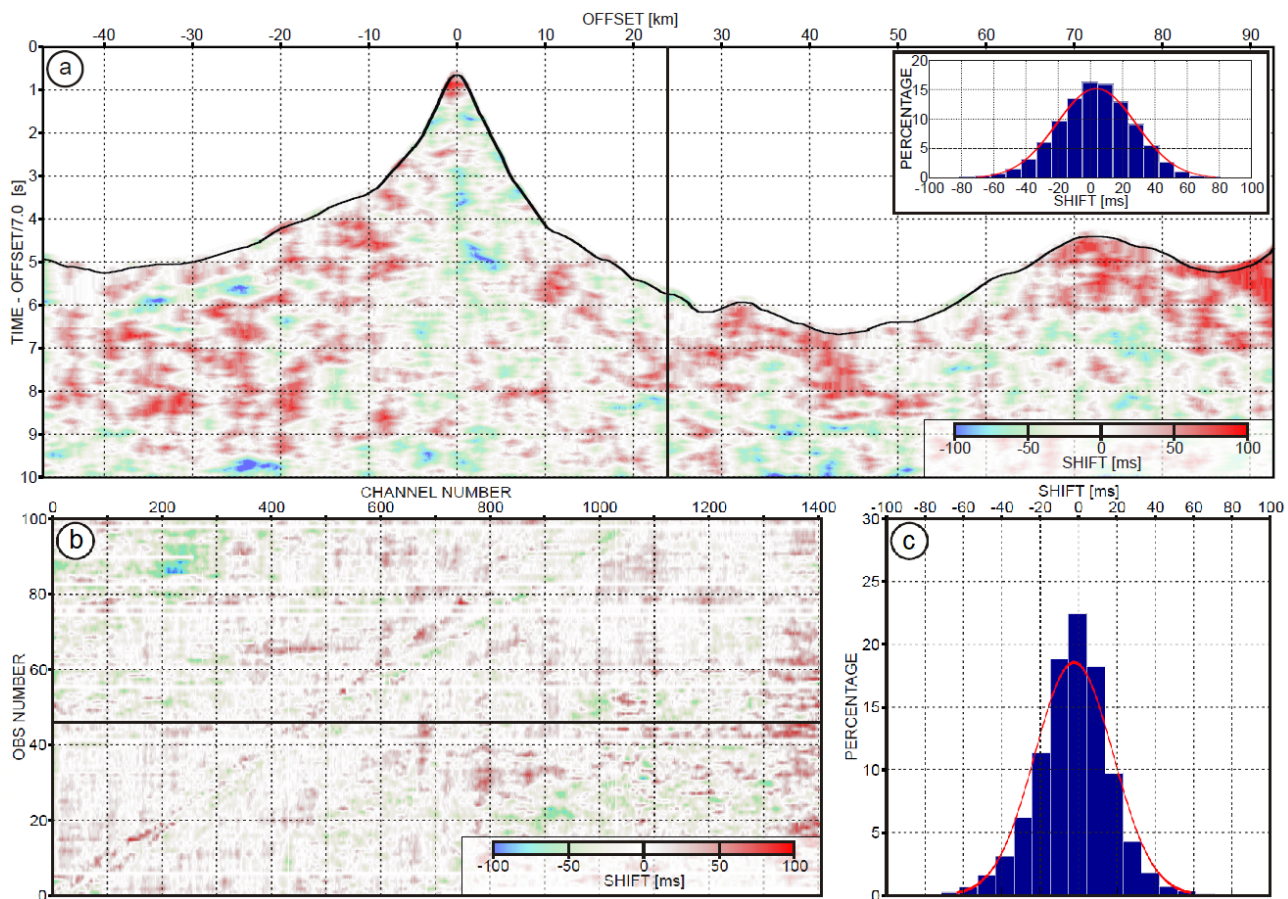
Figure 2: Illustration of DIW results. TOP: Map of the local shifts for all data samples in single OBS gather, with their histogram and fitted distribution shown in the inset. The black curve represents the samples collected 100 ms after the first arrivals. BOTTOM LEFT: Map of the local shifts for data samples located 100 ms after first arrival extracted from all OBS gathers. BOTTOM RIGHT: Histogram and fitted distribution of the shifts presented in BOTTOM LEFT panel. From Górszczyk et al. (2017)
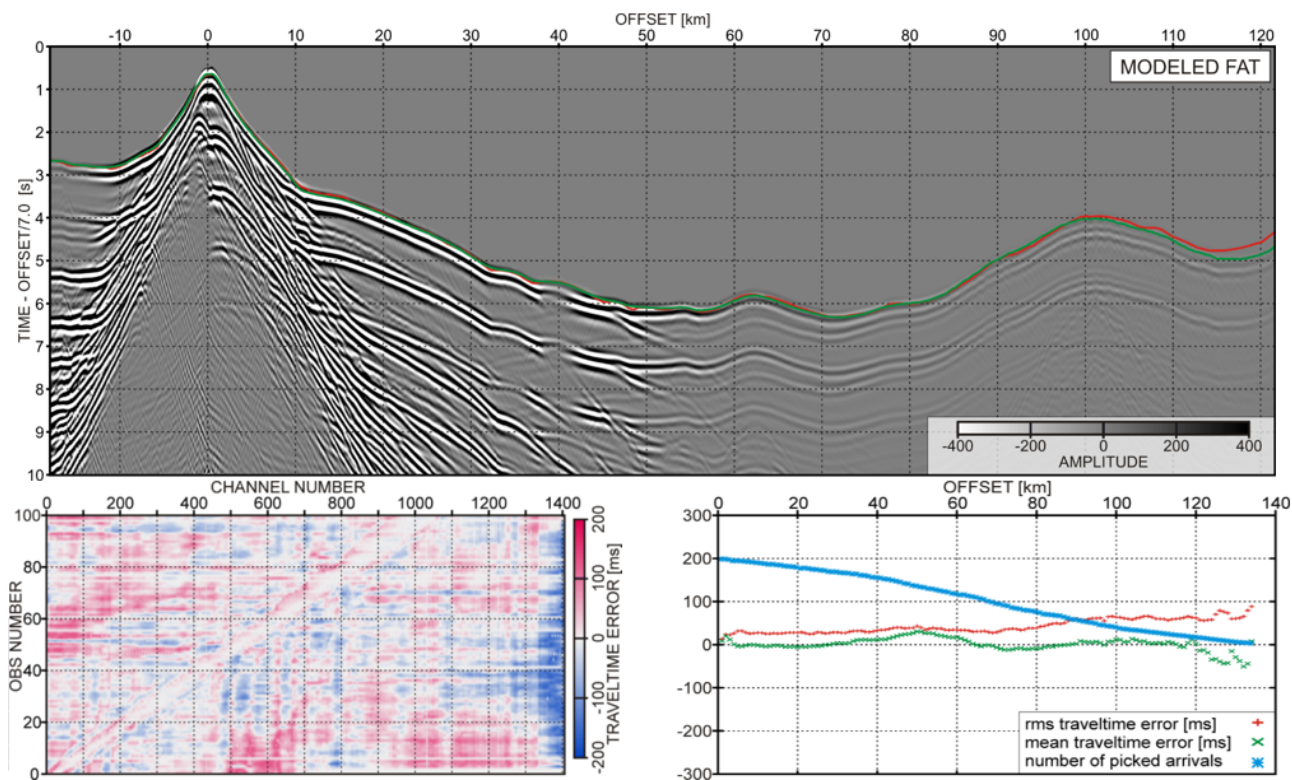
Figure 3: Assessment of the FAT model. TOP: Synthetic seismogram computed in the FAT model with superimposed picked (red line) and calculated (green line) traveltimes. BOTTOM LEFT: Traveltime difference map for all picked traces arranged in the source-vs-receiver coordinates. BOTTOM RIGHT: Mean traveltime difference and RMS (red + and green × respectively) calculated within 1-km offset intervals plotted against increasing offset. Cyan ∗ represent number of picked traces at given offset. From Górszczyk et al. (2017)
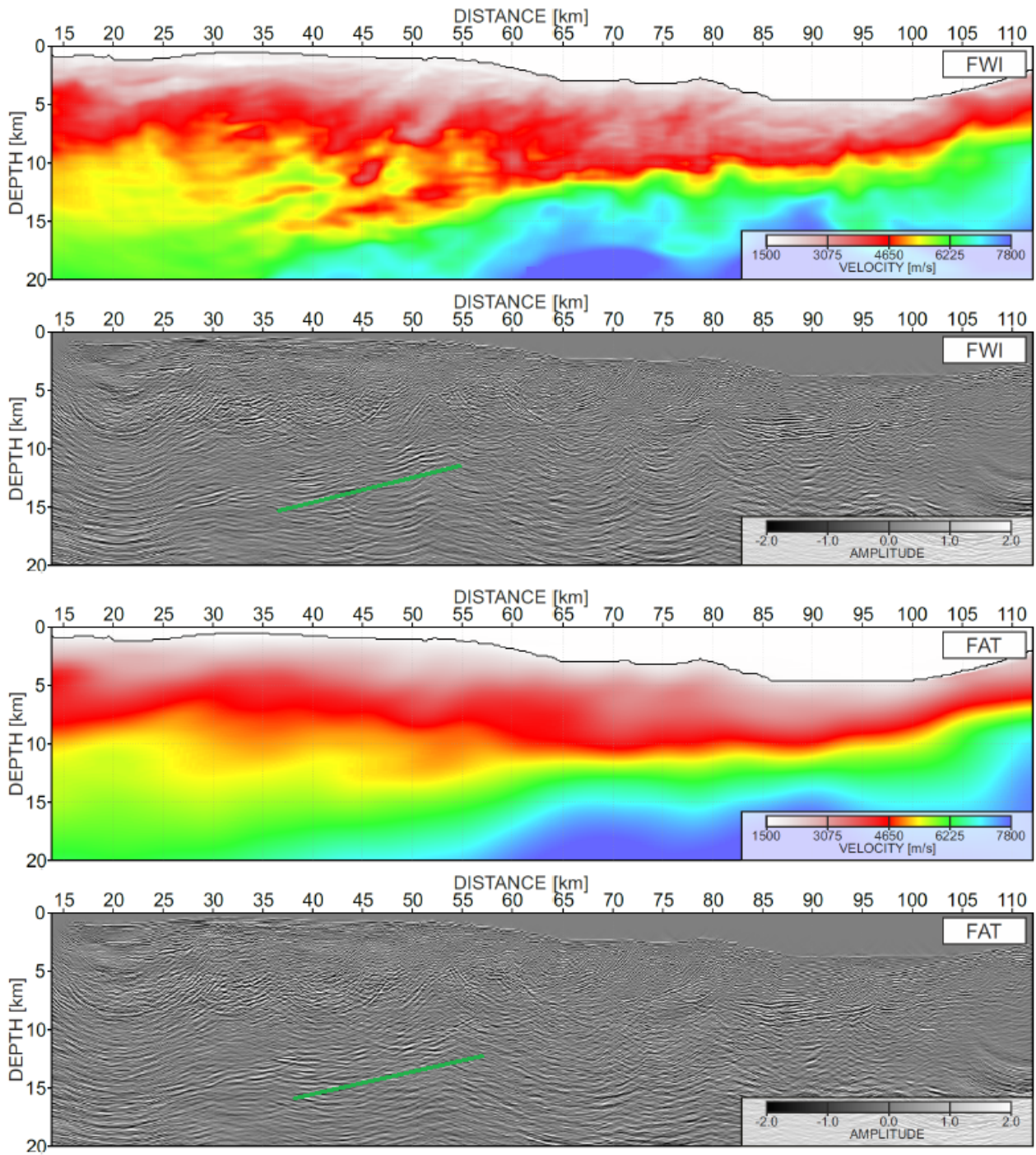
Figure 4: From the top to the bottom: FWI model and corresponding PSDM section derived from it; FAT model and corresponding PSDM section derived from it. Green line delineates better focusing of the interface in the PSDM section inferred from FWI model just below the LVZ.